

A PSO-Based Approach for Parameter Estimation in Synchronous Machines

Farid Leguebedj¹, Youcef Benmahamed¹,
Djamel Boukhetala², Kamel Boughrara¹

Abstract: This study employs the particle swarm optimization (PSO) approach using Stand Still Frequency Responses Testing (SSFR) to identify the time constants (poles and zeros) of the operational inductances along the d and q axes, as well as the parameters of the equivalent circuits for the SSFR1, SSFR2, and SSFR3 synchronous machine models. The difference between the frequency responses of the identified and simulated models at a standstill is minimized using a quadratic criterion in this method. The SSFR3 model accurately represents the synchronous machine, and simulation results show that the PSO approach is effective in terms of convergence rate and offers ideal solutions.

Keywords: Synchronous machine, Equivalent circuit, Parameters identification, Times constants, SSFR tests.

List of Symbols

s	Laplace's operator
V_d, V_q	d -axis stator voltage, q -axis stator voltage
i_d, i_q	d -axis current, q -axis current
V_f	d -axis field voltage
$L_d(s)$	d -axis operational inductance
$L_q(s)$	q -axis operational inductance
$G(s)$	is the stator to field transfer function

¹Laboratoire de Recherche en Electrotechnique (LRE), Ecole Nationale Polytechnique, Algiers, farid.leguebedj@g.enp.edu.dz, <https://orcid.org/0009-0005-5820-5177>; youcef.benmahamed@g.enp.edu.dz, <https://orcid.org/0000-0001-7179-3448>; kamel.boughrara@g.enp.edu.dz, <https://orcid.org/0000-0001-8379-7622>

²Laboratoire de Commande de Processus (LCP), Ecole Nationale Polytechnique, Algiers, djamel.boukhetala@g.enp.edu.dz, <http://orcid.org/0000-0003-2112-0709>

Colour versions of the one or more of the figures in this paper are available online at <https://sjec.ftn.kg.ac.rs>

L_d, L_q, L_f	d -axis synchronous inductance, q -axis synchronous inductance, field inductance
L_d, L_q	d -axis synchronous inductance, q -axis synchronous inductance
R_a, R_f	armature and field resistances
R_k, R_j	d -axis damper resistances
$R_{kq1}, R_{kq2}, R_{kq3}$	q -axis damper resistances
L_k, L_j	d -axis damper inductances
$L_{kq1}, L_{kq2}, L_{kq3}$	q -axis damper inductances
L_{md}	d -axis magnetizing inductance
L_{mq}	q -axis magnetizing inductance
L_a	leakage inductance
L_{amd}	the parallel combination of L_{md} and L_a
T'_{d0}, T'_d	d -axis transient open circuit and short-circuit time constant
T'_{q0}, T'_q	q -axis transient open circuit and short-circuit time constant
T''_{d0}, T''_d	d -axis sub-transient open circuit and short-circuit time constant
T''_{q0}, T''_q	q -axis sub-transient open circuit and short-circuit time constant
T'''_{d0}, T'''_d	d -axis sub-sub-transient open circuit and short-circuit time constant
T'''_{q0}, T'''_q	d -axis sub-sub-transient open circuit and short-circuit time constant

1 Introduction

Parameters identification of synchronous machines is crucial for analyzing both steady-state and transient performance of generating units [1]. Various computational methods have been utilized for this purpose in numerous studies [2, 3]. These studies primarily focus on characterizing two-axis models of synchronous machines through different testing approaches [4].

The accelerated evolutions of computer technology has enabled the development of various identification methods for synchronous generator models. These methods allow for the estimation of parameters during the machine's normal operation (on-line measurements) and are divided into two categories. Grey box modeling assumes a known model structure, such as orthogonal series [5, 6] or Kalman filters [7].

The second category, called “black box” modeling, does not presume any prior knowledge of the model structure. Instead, the goal is to establish the

relationship between the inputs and outputs of the system using techniques like neural networks [8, 9], Volterra series [10] or Hartley Series [11].

In [12], the most popular approach for determining the parameters of the d-q model using Standstill Frequency Response (SSFR) experiments was presented. The device stays stationary throughout SSFR tests, and the rotor is aligned along either the d-axis or the q-axis. A sinusoidal voltage of variable frequency is applied to two stator phases that are connected in series. An optimization procedure of the transfer function that represents the d-q model [2, 3] is then used to establish the parameters of the device.

The identification method recommended in IEEE Standard 115 [13] is the least squares method. This method focuses on reducing the weighted sum of errors between the transfer functions predicted by the chosen model and those determined via experimental measurements. The Levenberg-Marquardt and Gauss-Newton methods make it simple to implement and straightforward. But depending on the starting values and model selection, the outcome could converge to a local minimum, which is a major disadvantage. Maximum likelihood estimation [14, 15] and genetic algorithms [16, 17] are examples of more potent techniques.

Another approach for finding high-order equivalent circuits of synchronous machines using hybrid genetic algorithms is shown in [18]. Genetic algorithms (GAS) are successful at locating the global minimum within a search space and producing solutions that are independent of the initial values of the parameters. However, they require a lot of search time, which is not ideal for the online identification approaches mentioned in the literature [19].

The technique described in this paper is based on Particle Swarm Optimization (PSO). The initial algorithmic formulation [20] draws inspiration from the natural collective group behavior observed during the pursuit of food sources. This approach (PSO) is easier to implement and converges more quickly than Genetic Algorithms (GA), making it a popular choice for parameter identification [21, 22]. The results show that the PSO method converges quickly and accurately identifies optimal values.

The paper is structured as follows: Section 2 addresses operational quantities, Section 3 focuses on synchronous machine models, Section 4 covers particle swarm optimization, Section 5 details the Standstill Frequency Response test (SSFR), and Section 6 presents the PSO-based parameter identification method. Section 7 presents and discusses the simulation results of the PSO approach, while Section 8 concludes the paper.

2 Operational Quantities

Operational parameters can be modeled as transfer functions that define the connection between the rotor and stator terminals, treating the machine as a two-port network, as depicted in Fig. 1.

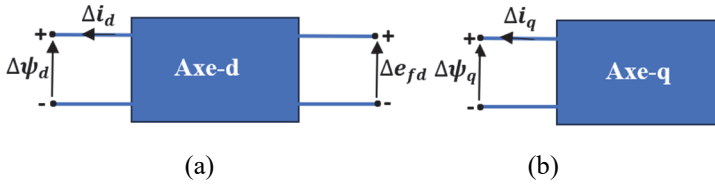


Fig. 1 – D-axis quadrupole and q-axis dipole.

The measurable quantities at the stator and rotor are related through a set of equations derived from the operational parameters. These operational parameters are then used to calculate the resistances and reactances of the machine windings. The following equations describe the stator flux [23]:

$$\Delta\psi_d(s) = G(s)\Delta e_{fd}(s) - L_d(s)\Delta i_d(s), \tag{1}$$

$$\Delta\psi_q(s) = -L_q(s)\Delta i_q(s). \tag{2}$$

3 Synchronous Machine Models

There are various models of synchronous machines, each characterized by the number of rotor circuits along the d and q axes. For example, the first-order model (SSFR1) includes an equivalent circuit with one excitation winding and one damper winding on the q axis.

The second-order model (SSFR2) has an equivalent circuit with one excitation winding, one damper winding on the d axis, and two damper windings on the q axis. Higher-order models (SSFR3) follow this structure, incorporating additional damper windings on the d and q axes as necessary.

Figs. 2 and 3 illustrate the 3rd order model along the d and q axes, respectively.

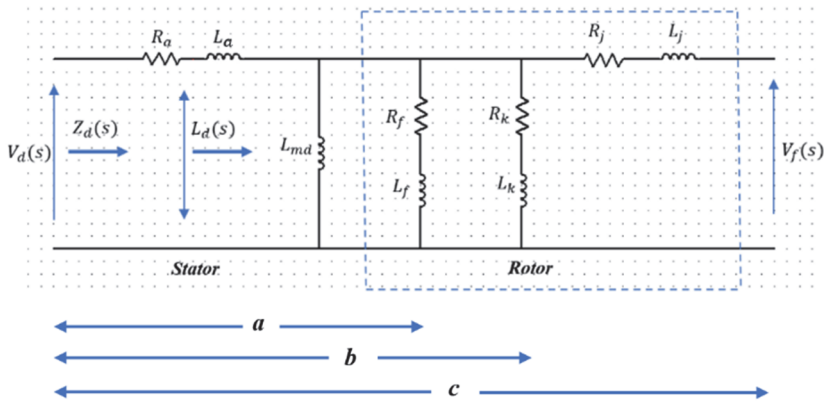


Fig. 2 – Equivalent Circuit of a third order model for d-axis (SSFR3).

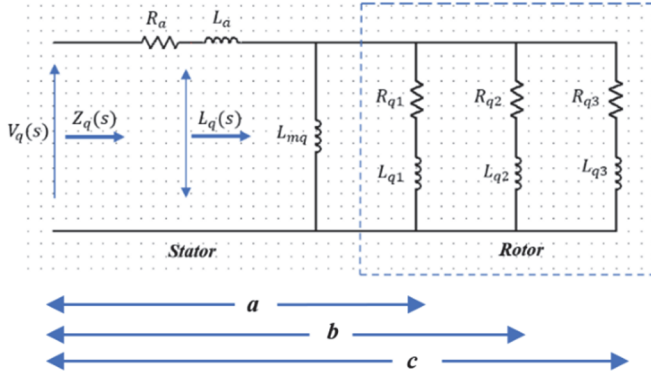


Fig. 3 – Equivalent Circuit of a third order model for q-axis (SSFR3).

3.1 First order model (SSFR1)

The first-order model's equivalent circuit is shown in Fig. 1a. The transfer function $L_d(s)$ for this circuit is computed using the formula below [24]:

$$L_d(s) = L_d \frac{1 + s \left(\frac{L_a L_{md} + L_a L_f + L_{md} L_f}{R_f L_d} \right)}{1 + \frac{L_{md} + L_f}{R_f}} \quad (3)$$

The standard form of (1) is:

$$L_d(s) = L_d \frac{1 + sT'_d}{1 + sT'_{d0}} \quad (4)$$

with:

$$L_{md} = L_d - L_a. \quad (5)$$

3.2 Second order model (SSFR2)

The operational inductance for the second-order model, which is stated as [24], is derived in Fig. 1b:

$$L_d(s) = L_d \frac{1 + s \left(\frac{L_f + L_{amd}}{R_f} + \frac{L_k + L_{amd}}{R_k} \right) + \frac{s^2 (L_f L_k + L_{amd})(L_k + L_{amdf})}{R_f R_k}}{1 + s \left(\frac{L_f + L_{md}}{R_f} + \frac{L_k + L_{md}}{R_k} \right) + \frac{s^2 (L_f L_k + L_{md})(L_k + L_{mdf})}{R_f R_k}}, \quad (6)$$

where L_{amd} is the parallel combination of L_{md} and L_a ; L_{amdf} is the parallel combination of L_{md} , L_f , L_a ; L_{mdf} is the parallel combination of L_{md} and L_f .

Equation (4) for operational inductance simplifies to:

$$L_d(s) = L_d \frac{1 + s(T'_d + T_1) + s^2 T'_d T''_d}{1 + s(T'_{d0} + T_2) + s^2 T'_{d0} T''_{d0}}, \quad (7)$$

with:

$$\begin{cases} T_1 = \frac{L_k + L_{amd}}{R_k} \\ T_2 = \frac{L_k + L_{md}}{R_k} \end{cases}, \quad (8)$$

The roots of the zero-pole from (5) are obtained by applying the quadratic formula to the numerator and denominator of $L_d(s)$. Regardless of the time constants, these roots have been proven to always be genuine. As a result, a second-order model may represent the operational inductance as follows:

$$L_d(s) = L_d \frac{(1 + sT'_d)(1 + sT''_d)}{(1 + sT'_{d0})(1 + sT''_{d0})}. \quad (9)$$

3.3 Third Order Model (SSFR3)

The third model's d-axis operational inductance may be expressed as follows:

$$L_d(s) = L_d \frac{1 + s \left(\frac{L_f + L_{amd}}{R_f} + \frac{L_k + L_{amd}}{R_k} \right) + \frac{s^2 (L_f L_k + L_{amd})(L_k + L_{amd})}{R_f R_k}}{1 + s \left(\frac{L_f + L_{md}}{R_f} + \frac{L_k + L_{md}}{R_k} \right) + \frac{s^2 (L_f L_k + L_{md})(L_k + L_{md})}{R_f R_k}} \quad (10)$$

The denominator is analogous to the numerator, with the substitution of L_{amd} for L_{md} in the coefficients of s , s^2 and s^3 .

$$Den = \frac{1}{R_f R_k R_j} \left[s^2 \left(\frac{L_f L_j + L_j L_{md} + L_f L_{md}}{R_f R_j} + \frac{L_j L_k + L_k L_{md} + L_j L_{md}}{R_j R_k} + \frac{L_f L_k + L_f L_{md} + L_k L_{md}}{R_k R_f} \right) + s^3 \frac{L_f L_k L_j + L_f L_k L_{md} + L_k L_j L_{md} + L_f L_j L_{md}}{R_f R_k R_j} \right], \quad (11)$$

then,

$$L_d(s) = \frac{Num}{Den}. \quad (12)$$

Consequently, the operational inductance for a third-order model is expressed by the formula:

$$L_d(s) = L_d \frac{(1 + sT'_d)(1 + sT''_d)(1 + sT'''_d)}{(1 + sT'_{d0})(1 + sT''_{d0})(1 + sT'''_{d0})}. \quad (13)$$

The proof of (3), (6) and (12) are given in Appendix A.

The equations for the operational inductance of the d-axis also apply to the q-axis.

4 Particle swarm optimization

Dr. Kennedy and Dr. Eberhart created the PSO algorithm, a powerful evolutionary approach influenced by the social behavior of animals like fish schools and bird flocks [26, 27]. In PSO, a collection of particles interacts with one another as they move arbitrarily across a search space [27, 28]. Every particle in the algorithm keeps in mind its own best answer as well as the best answer discovered by the entire swarm. Each particle updates its location in accordance with (14) using this information. The particle's velocity is changed during each iteration using the given formula.

$$v_{k+1} = w(k)v_k + c_1 \cdot r_1 + (lbp - cp_k) + c_2 \cdot r_2 (gp_k - cp_k). \quad (14)$$

The novel velocity is included in the present particle location (cp_k) to create the subsequent particle position (cp_{k+1}), as illustrated in (15).

$$cp_{k+1} = cp_k + v_{k+1}. \quad (15)$$

The value given to w , which stands for the inertia weight, was changed between the beginning and end values as follows:

$$w = (iter_{max} - iter_{cur}) \left(\frac{w_{initial} - w_{final}}{iter_{max}} \right) + w_{final}. \quad (16)$$

In this context, $w_{initial}$ and w_{final} represent the starting and ending inertia weights for a given run, respectively. The current iteration number at a given time step is represented by the phrase $iter_{cur}$, whereas the maximum number of iterations permitted in a run is represented by the term $iter_{max}$ [28].

The acceleration coefficients c_1 and c_2 are positive constants that represent the weights for individual and social influences that model the attractive forces toward the local and global best solutions, respectively. In most cases, c_1 and c_2 are in the range of 0 to 4 [26 – 28].

5 Standstill Frequency Response Test

The frequency response of stationary rotating machines is analyzed using the Stand-Still Frequency Response (SSFR) test. In recent years, the SSFR approach has emerged as one of the main standard methods for determining the dynamic characteristics of synchronous machines. The SSFR test determines the properties of operational quantities by examining their frequency dependence [25].

The rotor must be in two particular locations with relation to the stator because the SSFR technique necessitates that tests be carried out independently for the direct and quadrature axes. As recommended by IEEE Standard 115 [13], the experimental method for the SSFR test is shown in Fig. 4.

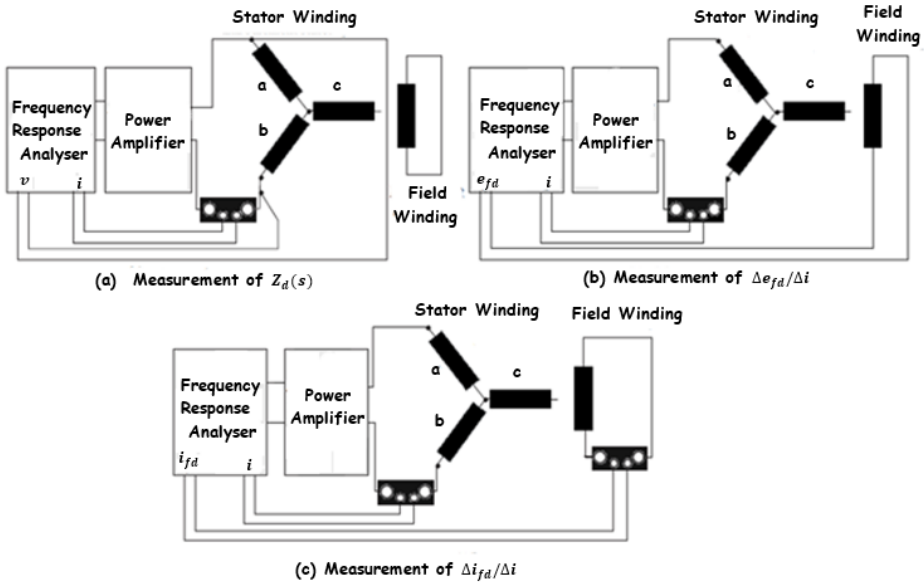


Fig. 4 – Protocol of SSFR tests according to the IEEE standard 115 A.

6 Implementation of the PSO Algorithm for Synchronous Machine Parameters Estimation

The core concept of using PSO algorithms for parameter identification is to transform the parameter estimation task into an *optimization* problem. In this approach, the unknown parameters are treated as particles within the algorithm. A performance function is then created to measure how closely the model's response matches the actual system response, and this function is optimized. The equation below defines the error between the measured data and the simulated model results [29]:

$$Error_i = Error_{Reai} + Error_{Imagi} \quad (17)$$

with:

$$Error_{Reai} = L_{dmi} \cos(\varphi_{mi}) - L_{di} \cos(\varphi_i), \quad (18)$$

$$Error_{Imagi} = L_{dmi} \sin(\varphi_{mi}) - L_{di} \sin(\varphi_i), \quad (19)$$

where:

L_{dmi} , φ_{mi} : are respectively the magnitude of the operational inductance and its phase measured experimentally.

L_{di} , φ_i : are, respectively, the magnitude of the simulated operational inductance and its phase.

The fitness function is defined as follows:

$$fitness = \frac{1}{N} \sum_{i=1}^N Error_i^2, \quad (20)$$

The length of the measured output vector is represented by N .

The simulated L_{di} expression for the SSFR1, SSFR2, and SSFR3 models is given by (2), (7), and (11) for time constants, and by (1), (4), and (10) respectively for the parameters of the equivalent circuits.

This study aims to identify the time constants of the SSFR1, SSFR2, and SSFR3 models, as well as the parameters of their equivalent circuits. The parameters to be identified for the first task are T'_d , T''_d , T'''_d , T'_{d0} , T''_{d0} , and T'''_{d0} , while for the second task, they include L_f , R_f , L_k , R_k , L_j , and R_j . The same procedure is used to identify parameters along the q axis.

The following procedures can be used to illustrate the suggested approach:

- Step 1: Under a variable frequency input, the system's response was measured.
- Step 2: Use the same inputs to the simulation as the real system.
- Step 3: Calculates the fitness of each particle (potential solutions).
- Step 4: Using the updating principles described in (14) and (15), update the potential solutions.
- Once the specified number of iterations has been reached or convergence has been achieved, the optimization process should be stopped. Otherwise, proceed to step 2.

7 Results and Discussions

The SSFR tests for a 250.02 MVA power machine at 16.5 kV, as published in EPRI reference [30], are utilized for both implementation and validation of the approach. The measured value of the synchronous inductance $L_d = 0.0045$ H and the leakage inductance $L_a = 8\%L_d$ given in the literature [25, 31].

The operational inductances along the axis and q-axis were selected as the optimization values due to their significant variability across a frequency range of 0.001 Hz to 1000 Hz. This enhances the optimization process by clearly highlighting the differences between measured data and model outputs. The SSFR test data and machine model results are then utilized to compute the output error.

The PSO was configured to optimize 2 variables (SSFR1), 4 variables (SSFR2), and 6 variables (SSFR3). These parameters are treated as particles in the Particle Swarm Optimization (PSO) algorithm. We set the swarm size (N) to 60 and the number of iterations to 150. For cognitive and social acceleration factors, we selected $c_1 = 2.0$ and $c_2 = 1.05$.

The random factors r_1 and r_2 are drawn at each iteration within the interval $[0, 1]$ to ensure diversity in particle positions and velocities. The fitness function, essential for evaluating the quality of proposed solutions, measures the mean square error between the measured data and the values simulated by the SSFR1, SSFR2, and SSFR3 models. The optimization results are discussed later.

7.1 Estimation of time constants and validation

We performed a number of numerical tests to evaluate how well the suggested approach identifies synchronous machine parameters. The performance criterion are as follows:

- The straightforward criterion of $J_d = J_{L_q}$ was employed to estimate the d-axis parameters.
- The straightforward criterion of $J_q = J_{L_d}$ was employed to estimate the q-axis parameters.

The time constants of the SFR 1, SSFR2, and SFR3 models along the d and q axes, obtained by the particle swarm optimization (PSO) approach, are presented in **Tables 1** and **2**, respectively.

To validate the results, the time constants along the q axis for the SSFR1, SSFR2, and SSFR3 models are introduced in (4), (9) and (13), respectively. This is achieved by substituting L_d with L_q and replacing the d-axis time constants ($T'_d, T''_d, T'''_d, T'_{d0}, T''_{d0}, T'''_{d0}$) with the q-axis time constants ($T'_q, T''_q, T'''_q, T'_{q0}, T''_{q0}, T'''_{q0}$).

Table 1

Estimation of d-axis time constants by the PSO approach.

Times Constants	SSFR1 model	SSFR2 model	SSFR3 model
$T'_d(s)$	0.6675	0.8151	0.8943
$T'_{d0}(s)$	3.6677	3.8489	3.9371
$T''_d(s)$	—	0.0057	0.0831
$T''_{d0}(s)$	—	0.0083	0.1068
$T'''_d(s)$	—	—	0.0025
$T'''_{d0}(s)$	—	—	0.0035

Table 2

Estimation of q-axis time constants by the PSO approach.

Times Constants	SSFR1 model	SSFR2 model	SSFR3 model
$T'_q(s)$	0.1198	0.5965	3.0267
$T'_{q0}(s)$	0.5936	1.4121	4.0898
$T''_q(s)$	—	0.0190	0.1612
$T''_{q0}(s)$	—	0.0561	0.0037
$T'''_q(s)$	—	—	0.0037
$T'''_{q0}(s)$	—	—	0.0083

Using the J_q criteria, the simulated and measured q-axis operational inductance magnitude and phase frequency responses are compared in Figs. 5 and 6.

Frequency zone comparison reveals three distinct zones:

a) Low frequency zone (10^{-2} Hz to 10^0 Hz)

For the magnitude:

- All curves start at the same magnitude level (~ -45 dB).
- The correspondence is good in this range, without significant deviations.

For the phase:

- Initially, all curves align with the experimental curve at 0 degrees phase.

b) Transition zone (10^0 Hz to 10^2 Hz)

For the magnitude:

- The experimental curve exhibits a gradual downward slope.
- PSO-SSFR1 shows a delayed transition, maintaining a higher magnitude before dropping sharply.

- PSO-SSFR2 aligns more closely with the initial slope but deviates slightly before reaching the measured curve.
- PSO-SSFR3 is the closest to the measured curve, though it also shows minor deviations.

For the phase:

- PSO-SSFR1 drops rapidly to -90° , which does not correspond to experimental reality.
- PSO-SSFR2 shows overly amplified oscillations.
- PSO-SSFR3 follows the general trend with good precision.

c) High frequency zone (10^2 Hz to 10^3 Hz)

For the magnitude:

- PSO-SSFR1 diverges significantly, exhibiting a higher magnitude than the measured curve.
- PSO-SSFR2 shares a similar slope but doesn't precisely align with the measured values.
- PSO-SSFR3 closely matches the measured curve.

For the phase:

- PSO-SSFR1 remains far from the measured curve.
- PSO-SSFR2 continues to oscillate excessively.
- PSO-SSFR3 remains the most faithful to the measured curve.

From the above, we conclude the following:

- PSO-SSFR3 is the most accurate model, closely matching the experimental curve across all frequency ranges.
- PSO-SSFR2 provides a reasonable approximation, though it is slightly less precise in the transition region.
- PSO-SSFR1 performs the worst, showing a delay in the transition and overestimating high-frequency magnitudes.

In conclusion, PSO-SSFR3 is the best model, minimizing deviations from the measured response throughout the spectrum.

Fig. 7 presents the evolution of the fitness function, which indicates that the identified parameters align closely with the actual values for the SSFR3 model.

For the SSFR1 model, the fitness function drops quickly and reaches the convergence requirement after 12 iterations; for the SSFR2 model, after 16 iterations; and for the SSFR3 model, after 14 iterations.

To avoid local minima and achieve the global minimum, we executed the PSO algorithm 50 successive times. As illustrated in Fig. 8, the error initially exhibits significant oscillations, indicating potential local minima traps.

However, over multiple iterations, PSO successfully navigates these challenges and converges to an optimal solution, thereby reducing global error despite the fluctuations. With this approach, the parameters of the synchronous generator may be determined with greater accuracy and stability.

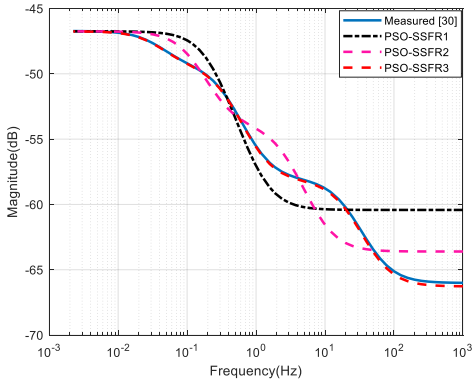


Fig. 5 – Operational inductance magnitude versus frequency (*q*-axis)

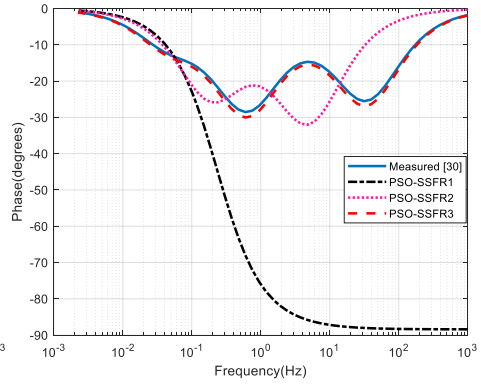


Fig. 6 – Operational inductance phase versus frequency (*q*-axis).

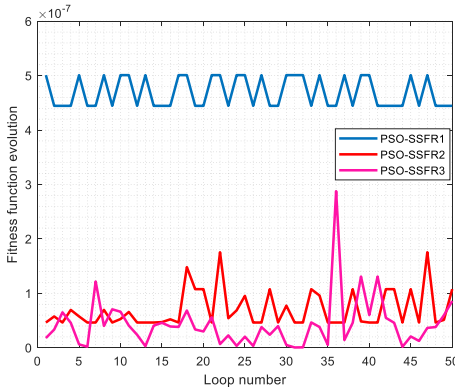


Fig. 7 – J_{Lq} Fitness function evolution (*q*-axis).

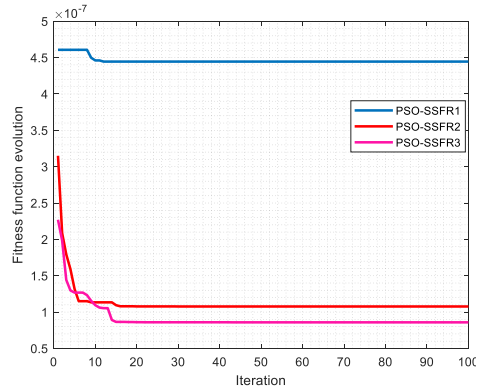


Fig. 8 – Fitness function evolution for 50 iterations.

7.2 Estimation of equivalent circuit parameters and validation

Tables 3 and 4 list the parameters of the equivalent circuits for models SSFR1, SSFR2, and SSFR3 along the *d* and *q* axes, which were determined using the PSO technique.

Table. 3

Estimation of d-axis equivalent circuit parameters by the PSO approach.

Parameters	SSFR1 model	SSFR2 model	SSFR3 model
L_f (mH)	0.552220	0.752950	0.792000
R_f (Ω)	0.001256	0.001400	0.001400
L_k (mH)	–	0.621430	0.542000
R_k (Ω)	–	0.152100	0.356200
L_j (mH)	–	–	1.800000
R_j (Ω)	–	–	0.025800

Table. 4

Estimation of q-axis equivalent circuit parameters by the PSO approach.

Parameters	SSFR1 model	SSFR2 model	SSFR3 model
L_{q1} (mH)	0.584900	3.400	10.50
R_{q1} (Ω)	0.007500	0.0052	0.0040
L_{q2} (mH)	–	0.37629	0.1490
R_{q2} (Ω)	–	0.0277	0.13240
L_{q3} (mH)	–	–	1.210
R_{q3} (Ω)	–	–	0.0100

In order to validate the results, one must take into account the transfer functions for operational inductance along the d-axis, which are described in Section 3, and include the estimated parameters of the equivalent circuits from models SSFR1, SSFR2, and SR3, as well as (3), (6) and (10).

Figs. 9 and 10 compare the frequency responses of the operational inductance magnitude and phase along the d-axis, identified using the J_{L_d} criterion and measured data.

For the magnitude (Fig. 9), we note:

- The experimental curve follows a gradual decay.
- PSO-SSFR1 shows an overestimation at high frequencies, moving away from the experimental reality.
- PSO-SSFR2 and PSO-SSFR3 follow the experimental curve better, with PSO-SSFR3 being the most accurate in the transition range.
- For the phase (Fig. 10) we note:
- The experimental curve shows a marked phase variation, with a pronounced minimum.
- PSO-SSFR1 diverges strongly after the minimum, overestimating the high-frequency phase.

- PSO-SSFR2 follows the general trend but with amplified oscillations.
- PSO-SSFR3 is the most faithful to the measured curve, especially after the transition frequency.

So, PSO-SFR3 is therefore the best candidate to represent the frequency response of operational inductance.

Fig. 11 depicts the progression of the fitness function, which shows that the parameters display a high degree of alignment with the measured values for the SSFR3 model.

The fitness function declines rapidly and reaches the convergence criteria after 12 iterations for the SSFR1 model, 28 iterations for the SSFR2 model, and 80 iterations for the SSFR3 model.

Fig. 12 shows the error from the PSO approach executed 50 consecutive times. Despite fluctuations, the PSO method successfully navigated these challenges and converged on an optimal solution.

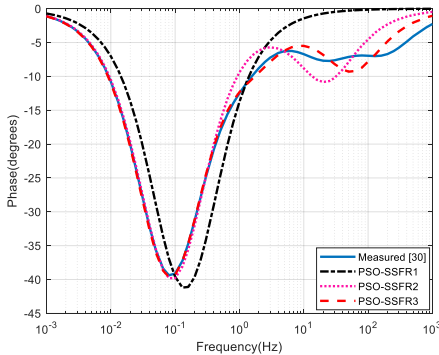


Fig. 9 – Operational inductance magnitude versus frequency (*d*-axis).

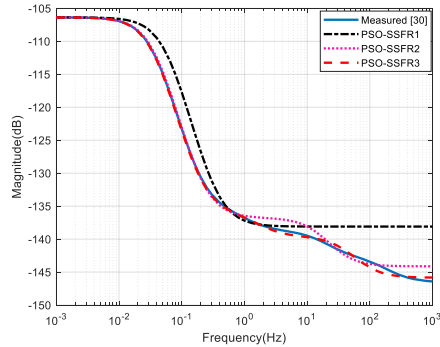


Fig. 10 – Operational inductance phase versus frequency (*d*-axis).

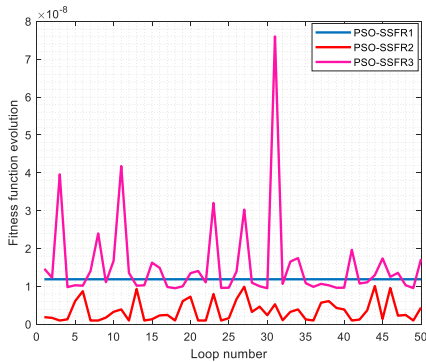


Fig. 11 – J_{L_d} Fitness function evolution (*d*-axis).

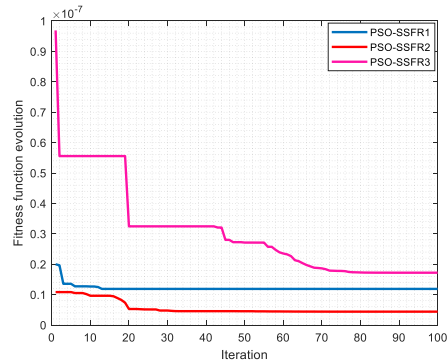


Fig. 12 – Fitness function evolution for 50 iterations (*d*-axis).

8 Conclusion

This paper proposes a particle swarm optimization (PSO) algorithm for identifying d-axis and q-axis operational inductance parameters. This approach is based on Stand Still Frequency Responses Testing conducted on a 250.02 MVA power generator with a voltage of 16.5 kV. The PSO algorithm effectively minimizes the quadratic criterion and accurately identifies the time constants and parameters of the d-axis and q-axis equivalent circuits for the SSFR1, SSFR2, and SSFR3 models, as demonstrated by simulation results. The obtained results indicate that the SSFR3 model emerges as the most efficient. Additionally, it is established that while the convergence time is negatively influenced by the number of parameters to be identified, the algorithm maintains its efficiency. As perspectives we recommend further research on the models' impact on the dynamic behavior of synchronous machines.

9 Appendix A

First order model (SSFR1)

$$\begin{aligned} sL_d(s) &= sL_a + \frac{sL_{md}(R_f + sL_f)}{sL_{md} + (R_f + sL_f)} \\ &= \frac{s^2L_aL_{md} + sL_aR_f + s^2L_aL_f + sL_{md}R_f + s^2L_{md}L_f}{R_f \left(1 + s \frac{L_f + L_{md}}{R_f} \right)} \end{aligned} \quad (A1)$$

with:

$$L_s = L_d - L_{md}, \quad (A2)$$

$$sL_d(s) = \frac{s^2L_aL_{md} + sL_dR_f - sL_{md}R_f + s^2L_aL_f + sL_{md}R_f + s^2L_{md}L_f}{R_f \left(1 + s \frac{L_f + L_{md}}{R_f} \right)} =$$

$$\frac{s^2L_aL_{md} + sL_dR_f + s^2L_aL_f + s^2L_{md}L_f}{R_f \left(1 + s \frac{L_f + L_{md}}{R_f} \right)} = \frac{sL_dR_f \left(1 + s \frac{L_aL_{md} + L_aL_f + L_{md}L_f}{L_dR_f} \right)}{R_f \left(1 + s \frac{L_f + L_{md}}{R_f} \right)}. \quad (A3)$$

$$L_d(s) = L_d \frac{\left(1 + s \frac{L_aL_{md} + L_aL_f + L_{md}L_f}{L_dR_f} \right)}{R_f \left(1 + s \frac{L_f + L_{md}}{R_f} \right)}. \quad (A4)$$

Second order model (SSFR2)

$$\begin{aligned}
 sL_d(s) &= sL_a + sL_{md} / / (R_f + sL_f) / / (R_k + sL_k) = \\
 &= \frac{sL_a + \frac{sL_{md}(R_f + sL_f)(R_k + sL_k)}{sL_{md}(R_f + sL_f) + sL_{md}(R_k + sL_k) + (R_f + sL_f)(R_k + sL_k)}}{sL_{md}(R_f + sL_f) + sL_{md}(R_k + sL_k) + (R_f + sL_f)(R_k + sL_k)} + \\
 &= \frac{sL_a \left[sL_{md}(R_f + sL_f) + sL_{md}(R_k + sL_k) + (R_f + sL_f)(R_k + sL_k) \right]}{sL_{md}(R_f + sL_f) + sL_{md}(R_k + sL_k) + (R_f + sL_f)(R_k + sL_k)} + \\
 &+ \frac{sL_{md}(R_f + sL_f)(R_k + sL_k)}{sL_{md}(R_f + sL_f) + sL_{md}(R_k + sL_k) + (R_f + sL_f)(R_k + sL_k)}.
 \end{aligned} \quad (A5)$$

Using, $L_{amd} = \frac{L_a L_{md}}{L_a + L_{md}}$, and $L_{amdf} = \frac{L_a L_{md} L_f}{L_a L_{md} + L_a L_f + L_f L_{md}}$, we substitute them into the numerator to obtain:

$$\begin{aligned}
 sL_d(s) &= \\
 &= \frac{1 + s \left(\frac{L_f + L_{amd}}{R_f} + \frac{L_k + L_{amd}}{R_k} \right) + \frac{s^2(L_f L_k + L_{amd})(L_k + L_{amdf})}{R_f R_k}}{1 + s \left(\frac{L_f + L_{md}}{R_f} + \frac{L_k + L_{md}}{R_k} \right) + \frac{s^2(L_f L_k + L_{md})(L_k + L_{mdf})}{R_f R_k}}.
 \end{aligned} \quad (A6)$$

Then:

$$L_d(s) = L_d \frac{1 + s \left(\frac{L_f + L_{amd}}{R_f} + \frac{L_k + L_{amd}}{R_k} \right) + \frac{s^2(L_f L_k + L_{amd})(L_k + L_{amdf})}{R_f R_k}}{1 + s \left(\frac{L_f + L_{md}}{R_f} + \frac{L_k + L_{md}}{R_k} \right) + \frac{s^2(L_f L_k + L_{md})(L_k + L_{mdf})}{R_f R_k}}. \quad (A7)$$

Third order model (SSFR3)

$$\begin{aligned}
 sL_d(s) &= sL_a + sL_{md} / / (R_f + sL_f) / / (R_k + sL_k) / / (R_j + sL_j) = \\
 &= \frac{sL_a + sL_{md} / / Z_f / / Z_k / / Z_j}{sL_{md} Z_f Z_k Z_j + sL_{md} Z_f Z_j + sL_{md} Z_k Z_j + Z_f Z_k Z_j}.
 \end{aligned} \quad (A8)$$

After development, we obtain:

$$\begin{aligned}
 L_d(s) &= \\
 &= \frac{sL_a Z_f Z_k Z_j + s^2 L_a Z_f Z_k L_{md} + s^2 L_a Z_f Z_j L_{md} + s^2 L_a Z_k Z_j L_{md} + sL_{md} Z_f Z_k Z_j}{sL_{md} Z_f Z_k + sL_{md} Z_f Z_j + sL_{md} Z_k Z_j + Z_f Z_k Z_j}.
 \end{aligned} \quad (A9)$$

To simplify the analysis, we examined the numerator and denominator separately.

$$\begin{aligned}
 Num = & \\
 & sL_a(R_f + sL_f)(R_k + sL_k)(R_j + sL_j) + sL_a(R_f + sL_f)(R_k + sL_k)sL_{md} + \\
 & sL_a(R_f + sL_f)(R_j + sL_j)sL_{md} + sL_a(R_k + sL_k)(R_j + sL_j)sL_{md} + \\
 & sL_{md}(R_f + sL_f)(R_k + sL_k)(R_j + sL_j).
 \end{aligned} \tag{A10}$$

Simplifying the previous expression yields:

$$\begin{aligned}
 Num = & s(L_a R_f R_k R_j) + \\
 & s^2 \left[L_a L_{md} (R_f R_k + R_f R_j + R_k R_j) + L_d (R_f R_k L_j + R_f R_k R_j + R_k R_j L_f) \right] + \\
 & s^3 \left[\begin{aligned} & L_a (R_f R_k L_j + R_f R_k R_j + R_k R_j L_f) + \\ & L_a L_{md} (R_f L_k + R_f L_j + R_k L_f + R_j L_f + R_j L_k) \\ & L_{md} (R_f L_k L_j + R_k L_f L_j + R_j L_f L_k) \end{aligned} \right] + \\
 & s^4 (L_a L_f L_k L_j + L_f L_k L_j).
 \end{aligned} \tag{A11}$$

Using,

$$L_{amd} = \frac{L_a L_{md}}{L_a + L_{md}}, \tag{A12}$$

we substitute this into the numerator, factor out $s(L_a + L_{md})$, and divide the equation by $R_f R_k R_j$ to obtain the following expression:

$$N_{um} = \frac{(L_a + L_{md})}{R_f R_k R_j} \left[\begin{aligned} & 1 + s \left(\frac{L_f + L_{amd}}{R_f} + \frac{L_k + L_{amd}}{R_k} + \frac{L_j + L_{amd}}{R_j} \right) + \\ & s^2 \left(\frac{L_f L_j + L_j L_{amd} + L_f L_{amd}}{R_f R_j} + \frac{L_j L_k + L_k L_{amd} + L_j L_{amd}}{R_j R_k} + \right. \\ & \left. \frac{L_f L_k + L_f L_{amd} + L_k L_{amd}}{R_k R_f} \right) + \\ & s^3 \frac{L_f L_k L_j + L_f L_k L_{amd} + L_k L_j L_{amd} + L_f L_j L_{amd}}{R_f R_k R_j} \end{aligned} \right] \tag{A13}$$

The denominator ‘‘Den’’ mirrors the numerator’s structure, substituting L_{amd} with L_{md}

$$Den = \frac{1}{R_f R_k R_j} \left[\begin{array}{l} 1 + s \left(\frac{L_f + L_{md}}{R_f} + \frac{L_k + L_{md}}{R_k} + \frac{L_j + L_{md}}{R_j} \right) + \\ s^2 \left(\frac{L_f L_j + L_j L_{md} + L_f L_{md}}{R_f R_j} + \frac{L_j L_k + L_k L_{md} + L_j L_{md}}{R_j R_k} + \right. \\ \left. \frac{L_f L_k + L_f L_{md} + L_k L_{md}}{R_k R_f} \right) + \\ s^3 \frac{L_f L_k L_j + L_f L_k L_{md} + L_k L_j L_{md} + L_f L_j L_{md}}{R_f R_k R_j} \end{array} \right] \quad (A14)$$

Then:

$$L_d(s) = \frac{Num}{Den} . \quad (A15)$$

10 References

- [1] E. da Costa Bortoni, J. A. Jardini: Identification of Synchronous Machine Parameters Using Load Rejection Test Data, IEEE Transactions on Energy Conversion, Vol. 17, No. 2, June 2002, pp. 242 – 247.
- [2] T. Kano, H. Nakayama, T. Ara, T. Matsumura: A Calculation Method of Equivalent Circuit Constants with Mutual Leakage Reactance on Synchronous Machine with Damper Winding, IEEE Transactions on Industry Applications, Vol. 127, No. 7, July 2007, pp. 761 – 766.
- [3] T. Zanma, T. Kawamura, M. Ishida: Calculation of Parameters of Equivalent Circuit of Permanent Magnet Synchronous Motor Using PSO with Grouped Agents, IEEE Transactions on Industry Applications, Vo. 127, No. 7, July 2007, pp. 731 – 738.
- [4] A. Hassannia, A. Darabi, and M. Alshamali: Estimation of Dynamic Parameters of a Synchronous Generator Using Genetic Algorithm, IEEE Transactions on Electrical and Electronic Engineering, Vo. 4, No. 5, September 2009, pp. 668 – 673.
- [5] J. J. R. Melgoza, G. T. Heydt, A. Keyhani, B. L. Agrawal, D. Selin: An Algebraic Approach for Identifying Operating Point Dependent Parameters of Synchronous Machines Using Orthogonal Series Expansions, IEEE Transactions on Energy Conversion, Vol. 16, No. 1, March 2001, pp. 92 – 98.
- [6] J. J. R. Melgoza, G. T. Heydt, A. Keyhani, B. L. Agrawal, D. Selin: Synchronous Machine Parameter Estimation Using the Hartley Series, IEEE Transactions on Energy Conversion, Vol. 16, No. 1, March 2001, pp. 49 – 54.
- [7] H. G. Aghamolki, Z. Miao, L. Fan, W. Jiang, D. Manjure: Identification of Synchronous Generator Model with Frequency Control Using Unscented Kalman Filter, Electric Power Systems Research, Vo. 126, September 2015, pp. 45 – 55.
- [8] O. Shariati, M. R. Aghamohammadi, B. Potter: On-Line Determination of Salient-Pole Hydro Generator Parameters by Neural Network Estimator Using Operating Data (PEANN), IEEE Access, Vol. 9, September 2021, pp. 134638 – 134648.

- [9] M. Calvo, O. P. Malik: Synchronous Machine Steady-State Parameter Estimation Using Neural Networks, *IEEE Transactions on Energy Conversion*, Vol. 19, No. 2, June 2004, pp. 237 – 244.
- [10] R. D. Fard, M. Karrari, O. P. Malik: Synchronous Generator Model Identification for Control Application Using Volterra Series, *IEEE Transactions on Energy Conversion*, Vol. 20, No. 4, December 2005, pp. 852 – 858.
- [11] J. J. R. Melgoza, G. T. Heydt, A. Keyhani, B. L. Agrawal, D. Selin: Synchronous Machine Parameter Estimation Using the Hartley Series, *IEEE Transactions on Energy Conversion*, Vol. 16, No. 1, March 2001, pp. 49 – 54.
- [12] F. S. Sellschopp, M. A. Arjona-Lopez: An Automated System for Frequency Response Analysis with Application to an Undergraduate Laboratory of Electrical Machines, *IEEE Transactions on Education*, Vol. 47, No. 1, February 2004, pp. 57 – 64.
- [13] Institute of Electrical and Electronics Engineers, author, issuing body: 115-2019 - IEEE Guide for Test Procedures for Synchronous Machines Including Acceptance and Performance Testing and Parameter Determination for Dynamic Analysis, New York: IEEE, New York, 2020.
- [14] R. Wamkeue, I. Kamwa, X. Dai-Do, A. Keyhani: Iteratively Reweighted Least Squares for Maximum Likelihood Identification of Synchronous Machine Parameters from On-Line Tests, *IEEE Transactions on Energy Conversion*, Vol. 14, No. 2, June 1999, pp. 159 – 166.
- [15] A. Belqorchi, U. Karaagac, J. Mahseredjian, I. Kamwa: Standstill Frequency Response Test and Validation of a Large Hydrogenerator, *IEEE Transactions on Power Systems*, Vol. 34, No. 3, May 2019, pp. 2261 – 2269.
- [16] B. B. Firouzi, E. Jamshidpour, T. Niknam: A New Method for Estimation of Large Synchronous Generator Parameters by Genetic Algorithm, *World Applied Sciences Journal*, Vol. 4, No. 3, 2008, pp. 326 – 331.
- [17] G. Kalarikovilagam Srinivasan, H. Thilagar Srinivasan: In Situ Parameter Estimation of Synchronous Machines Using Genetic Algorithm Method, *Advances in Electrical and Electronic Engineering*, Vol. 14, No. 3, September 2016, pp. 254 – 266.
- [18] T. Niewierowicz, R. Escarela-Perez, E. Campero-Littlewood: Hybrid Genetic Algorithm for the Identification of High-Order Synchronous Machine Two-Axis Equivalent Circuits, *Computers & Electrical Engineering*, Vol. 29, No. 4, June 2003, pp. 505 – 522.
- [19] M. Hasni, O. Touhami, R. Ibtouen, M. Fadel, S. Caux: Estimation of Synchronous Machine Parameters by Standstill Tests, *Mathematics and Computers in Simulation*, Vol. 81, No. 2, October 2010, pp. 277 – 289.
- [20] P. Kou, J. Zhou, C. Wang, H. Xiao, H. Zhang, C. Li: Parameters Identification of Nonlinear State Space Model of Synchronous Generator, *Engineering Applications of Artificial Intelligence*, Vol. 24, No. 7, October 2011, pp.1227 – 1237.
- [21] M. R. Alrashidi, M. E. El-Hawary: A Survey of Particle Swarm Optimization Applications in Power System Operations, *Electric Power Components and Systems*, Vol. 34, No. 12, 2006, pp. 1349 – 1357.
- [22] L. Liu, W. Liu, D. A. Cartes: Particle Swarm Optimization-Based Parameter Identification Applied to Permanent Magnet Synchronous Motors, *Engineering Applications of Artificial Intelligence*, Vol. 21, No. 7, October 2008, pp. 1092 – 1100.
- [23] P. Kundur: *Power System Stability and Control*, McGraw-Hill, New York, San Francisco, 2007.

A PSO-Based Approach for Parameter Estimation in Synchronous Machines

- [24] F. Leguebedj, D. Boukhetala, M. Tadjine: An Optimization Analytical Method for Synchronous Machine Model Design from Operational Inductance $L_d(s)$, Progress In Electromagnetics Research B, Vol. 97, November 2022, pp. 115 – 130.
- [25] A. Walton: A Systematic Method for the Determination of the Parameters of Synchronous Machines from the Results of Frequency Response Tests, IEEE Transactions on Energy Conversion, Vol. 15, No. 2, June 2000, pp. 218 – 223.
- [26] B. Tonsic Araujo, J. V. Bernardes Jr., E. da Costa Bortoni, G. Lambert-Torres: Synchronous Machine Parameters Evaluation with a Hybrid Particle Swarm Optimization Algorithm, Electric Power Components and Systems, Vol. 45, No. 17, 2017, pp.1962 – 1971.
- [27] I. Pan, S. Das: Fractional Order Fuzzy Control of Hybrid Power System with Renewable Generation Using Chaotic PSO, ISA Transactions, Vol. 62, May 2016, pp. 19 – 29.
- [28] A. Lari, A. Khosravi, F. Rajabi: Controller Design Based on μ Analysis and PSO Algorithm, ISA Transactions, Vol. 53, No. 2, March 2014, pp. 517 – 523.
- [29] B. Elrachid, R. Hammoud, B. Oussama: Parameters Identification of Synchronous Machine Based on Particle Swarm Optimization, E3S Web of Conferences, Vol. 336, January 2022, p. 00052.
- [30] N. E. I Parsons: Compendium of the EPRI Workshop on Determination of Synchronous Machine Stability Study Constants, Electric Power Research Institute, August 1980.
- [31] A. Walton: Characteristics of Equivalent Circuits of Synchronous Machines, IEE Proceedings -Electric Power Applications, Vol. 143, No. 1, January 1996, pp. 31 – 40.